Analysis & Optimization of Wire-EDM Parameters for Dimensional Stability of AZ91 Based Al_2O_{3p}/SiC_p Hybrid Composite

Dheeraj Kumar [a*], Rajesh Kumar Porwal [b]

[a] *Research Scholar, Faculty of Mechanical Engineering, Institute of Technology, SRMU Lucknow, U.P., India*

[b] *Professor, Faculty of Mechanical Engineering, Institute of Technology, SRMU, Lucknow, U.P., India*

[a]dheerajkr18@gmail.com, [b]porwal.me@srmu.ac.in

ARTICLE INFO

Keywords:

AZ91;
Top Kerf Width;
Bottom Kerf Width;
Taper Angle;
MMC;

ABSTRACT

The present work focuses on the primary objectives to analyse the dimensional stability of machined samples through kerf width and taper angle. Further to optimize the process parameters to obtain optimum results. The RSM-BBD approach has been used to design the experiments. Mg-based metal matrix hybrid composite samples were prepared using the stir casting process. Prepared samples are machined on a CNC wire-cut EDM. Matrix of Mg alloy AZ91 (94%) and reinforcement of SiC (4%) and Al_2O_3 (2%) powder is selected. Machined samples are observed for kerf width and taper angle calculations, followed by the optimization of process parameters to obtain optimum kerf width and taper angle. An optical microscope is used to measure the kerf width with 10x magnification. Top kerf width (T_{kw}), bottom kerf width (B_{kw}), and taper angle have been calculated, and a parametric plot is shown. Results obtained show that pulse on time and current is most significant factors in obtaining the optimum values of output responses. Optimum values of top kerf width and bottom kerf width are obtained at T_{on} = 18µs, T_{off} = 5µs, I = 3A & WS = 10.4m/s, and T_{on} = 18µs, T_{off} = 9µs, I = 3A & WS = 3.12m/s, respectively. Optimum value of taper angle is obtained at T_{on} = 30µs, T_{off} = 7µs, I = 3A & WS = 10.4m/s.

1. Introduction

Over the years, the demands for materials with specific characteristics have changed in the field of the aerospace industry. It eventually leads to the development of smart materials and composites. It drew attention to lightweight materials with excellent specific properties. Machinability and development of intricate shapes were focussed for the material selection. Geometrical accuracy of the parts are concerned and given priority to meet the dimensional satisfaction. Magnesium and its alloys are widely used for the structural framework despite being lightweight. Pure magnesium has high reactivity with the open atmosphere; therefore, its uses are limited. Reinforced magnesium has outstanding properties like lower density, greater strength, higher damping limits, exemplary fluidity for casting, non-magnetism, satisfactory heat conduction, good elastic shielding effect, lower heat capacity, and negative electrochemical potential. It is recyclable and nontoxic as well.

The significance of the composite lies in its improved properties compared to the pure matrix material. Composites are defined as a composition of two or more metals having matrix and the other as reinforcement. The variation of reinforcement relies on the desired outcome in material characteristics. Composite materials are made up of a matrix phase that has metallic compounds, metals in fibre or powder form, and ceramic particles or oxides acting as reinforcement. Although insoluble, the material phases exhibit strong adhesion at their interfaces. Better qualities that are challenging to get singly with polymers, metals, or ceramics are provided by it. Machining of composites has been a cumbersome task with the conventional methods. For cutting intricate shapes and difficult-to-machine materials, wire electric discharge machining has proved its versatility amongst all. Wire Electric Discharge Machining (WEDM) is an electrothermal method that removes material from the workpiece by successive sparks between the wire electrode and the sample workpiece in an intermediate dielectric fluid. During this process, the wire does not come in contact with the workpiece; dielectric fluid is used to flush away the debris, and the material of the wire can be brass, molybdenum, copper, tungsten, or steel core wire. It may be a coated type or diffusion annealed.

Arif U. et al. developed a thermal model and optimized spark erosion machining parameters for aluminium-based hybrid composites reinforced with SiC. Their work used a constant 10% SiC_{micro} reinforcement while varying SiC_{nano} content at three levels (3%, 4.5%, and 6%). The study revealed that Shabdard's Fc function provided the most accurate predictions for material removal rate (MRR) and surface roughness (SR). Further optimization using ANOVA validated the reliability of this model [27]. In a related study, Umair Arif et al. employed a Gaussian heat source to simulate

spark energy distribution and spark radius in Al-10% SiC_{micro}-SiC_{nano} composites. They concluded that pulse current was the most significant parameter influencing both MRR and SR, followed by T_{on} and nanoparticle percentage [28].

Ishfaq et al. investigated geometrical accuracy in WEDM of Al 6061, with a focus on angular deviations on the upper and lower surfaces of the machined workpiece. They reported that flushing pressure, wire tension, and T_{off} strongly influenced upper-face deviation, while V_{open}, T_{on}, flushing pressure, and wire feed primarily controlled the lower-face deviation [1]. Similarly, Muthukumar et al. optimized WEDM of Incoloy-800 and achieved a high MRR of 0.0576g/min, a low R_a of 3.10µm, and a kerf width (K_w) of 0.296mm under conditions of 50V gap voltages, 10µs T_{on}, 6µs T_{off}, and 8mm/min wire feed [2]. These results emphasized the need for careful tuning of electrical and mechanical parameters for dimensional accuracy.

R. Naveed et al. studied the machining of W-Co composites using zinc-coated wire in WEDM, successfully generating complex taper geometries. They demonstrated that with optimized settings, angular distortion could be limited to 0.16° and radial distortion to 6mm, corresponding to 33.3% and 14.3% reductions compared to baseline conditions [3]. Farooq et al. also proposed an innovative flushing mechanism for Inconel 718, reducing angular and radial deviations by 8.24% and 29.11%, respectively, while maintaining spark gap stability [10]. Complementary works by Shah et al. and Lakshmanan et al. confirmed that T_{on} and discharge current are dominant parameters influencing K_w, with higher current improving melting efficiency but also increasing kerf [12 & 14].

Hybrid and advanced machining techniques have also shown promise. Xiaoyu et al. combined fixed abrasive diamond wire saw technology with WEDM to propose a hybrid machining method. Their results indicated lower R_a and K_w compared to conventional WEDM, while eliminating recast layers and heat-affected zones [4]. Similarly, Hynes et al. optimized abrasive water jet machining of SiC, reporting that medium traverse speeds yielded a balance of good R_a and high productivity, and thinner SiC plates resulted in smaller taper angles [5]. Kolli et al. employed RSM-TOPSIS for multi-objective optimization of abrasive aqua jet machining of Al7075 MMC, where water pressure and stand-off distance emerged as key factors, achieving MRR = 4.87mm^3/min, R_a = 3.57µm, and a taper angle reduction of nearly 50% compared to single-variable optimization [15].

Kerf width prediction and accuracy control were addressed in several works. Baliarsingh and Samantaray showed that voltage and pulse duration significantly influenced cut-width in polymer composites [6]. Majumdar and Maity applied GRNN and MRA for WEDM of Ti grade-6, finding prediction errors of 5% and 10%, respectively, with GRNN proving superior for estimating K_w, R_a, and MRR [9]. Kumar et al. advanced optimization of AISI P20+Ni machining using cryo-treated zinc-coated brass wire, achieving K_w = 0.269mm, MRR = 2.72mm^3/min, and SR = 3.27µm, with validation through RSM and a deep-belief neural network hybrid approach [20]. These studies demonstrate the increasing role of machine learning in process parameter optimization.

Research on EDM of Mg- and Ti-based composites has further expanded understanding. Mustu et al. examined powder-mixed EDM of TiB_2 and TiB_2 + Nano-graphene reinforced ZK60 Mg alloys, identifying processing duration as the most influential parameter (87.58%), followed by current (3.2%). They showed that additive-reinforced ZK60 alloys exhibited improved machinability and surface quality [31]. Das et al. evaluated the machinability of Mg/TiC composites, finding T_{on} as the most critical factor for SR (79% contribution) and MRR (34%) [32]. Similarly, Ammisetti et al. optimized EDM of AZ91/Gr/Al_2O_3 composites using a hybrid ANN-TLBO model, achieving ±10% prediction accuracy for MRR and SR [33].

Optimization of EDM and WEDM parameters for AZ91 alloys was also addressed. Urtekin et al. found that Ton strongly influenced both MRR and SR, with higher Ton increasing removal rates but deteriorating surface finish, while shorter T_{on} improved SR but lowered MRR. T_{off} and wire feed had secondary effects [34]. Aruna et al. reinforced AZ91 with 3 wt.% Al_2O_3 and 2–6 wt.% SiC, achieving a fine grain size of 25µm, density of 1.946 g/cm^3, porosity <1%, hardness of 98 HV, toughness of 16.4 J/mm^2, and tensile strength of 352MPa [41]. Ge et al. strengthened SiCp/AZ91 brazed joints through Ti addition, enhancing filler wettability and improving shear strength by 43.4% [42].

Kerf width optimization has been identified as a critical challenge in machining high-performance alloys. Pramanik et al. showed that in Ti6Al4V, K_w increases with higher pulse rate and decreases with shorter T_{on} and higher wire tension [16]. Singh et al. identified discharge current as the dominant factor for K_w in Nimonic-80A machining [17], while Moharana et al. used Taguchi and utility approaches to simultaneously minimize K_w and maximize MRR and R_a [18]. Thiagarajan et al. reinforced Al6061 hybrid composites with nano SiC and ZrO_2, reporting that K_w decreased with T_{off} but increased with T_{on} and gap voltage [19].

The literature review carried out reveals that researchers have utilized unconventional machining to machine hard materials. They

found EDM and Abrasive Water Jet Machining very useful to minimize the geometrical error in the machined part. All the papers studied have worked with Al, WC, SiC, and other materials. The literature review presented showed that magnesium alloys and their composites are considered for performance analysis using EDM parameters. Mg reinforced with Al_2O_3 and SiC have been developed with the stir casting method and examined for optimized machining parameters for MRR and SR, but less work has been observed for dimensional accuracy in hybrid composites. It sparked a desire to work on the Hybrid magnesium metal matrix composite. The present work has used AZ91 Mg Alloy as the matrix material and SiCp and Al_2O_3p as reinforcement. Samples were developed using the stir casting method. WEDM was used to machine the samples using Molybdenum wire as the tool material. Kerf Width (Top Face and Bottom Face) and Taper Angle of the cut slot have been measured and analysed.

2. Processing of Materials and Methods

2.1 Development of Magnesium Metal Matrix Composites (MMMCs):

In the present study, magnesium alloy AZ91 was selected as the matrix material for the MMMC. The following Table 01 shows the compositions and physical properties of AZ91. These properties are major influencing factors behind the wide application of AZ91 in the automotive components and structural applications. Table 02 shows the physical & chemical properties of reinforced materials SiC and Al_2O_3.

An electronic weighing balance with a calibration of 0.1 g was utilized to measure the fractional weight of the pure alloy AZ91 and reinforcement material before melting. For making the sample 329gm (94%) of AZ91, 14gm (4%) of SiC, and 7gm (2%) of Al_2O_3 by weight were used.

Table-01 Compositions & properties of magnesium alloy AZ91

Compositions of AZ91		Physical Properties of AZ91	
Ele-ment	Weight %	Properties	Values at room Temp.
Al	8.30%	Density	1.81 gm/cm^3
Mn	0.20%	Tensile Strength	240-250 MPa
Zn	1.0%	Yield Strength	160 MPa
Si	0.10%	Melting Point	421^{0}C
Cu	0.03%	Purity	99.90%
Fe	0.01%		
Mg	Balance		

Magnesium alloy AZ91 was cut into small pieces by a power hexa cutter for the suitability of melting. In house set up of stir casting, embedding gas fired furnace, has been developed at the institute's laboratory. A stainless steel rod of 10 mm diameter was used as a stirrer. One end was connected to an electric motor, while the other end was connected to a hexagonal shape for turbulent creation. Since magnesium is very reactive to the open environment, an inert gas (Argon) was used to create protective shielding from atmospheric oxygen. Inert gas was also used during the casting into the mold. A digital thermocouple is used to monitor the temperature of the furnace. Pre-heated reinforcement material, Silicon carbide powder (SiC) 4% by weight, and Aluminium oxide powder (Al_2O_3) 2% by weight are mixed with molten metal. A metallic mold was used to cast the composite material. Figure 01 shows the schematic diagram of in house developed stir casting setup.

Table-02 Physical & chemical properties of SiC & Al_2O_3

Physical & Chemical Properties of SiC		Physical & Chemical Properties of Al_2O_3	
Properties	Values at room temperature	Properties	Values at room temperature
Density	3.21 gm/cm^3	Density	3.95 gm/cm^3
Melting Point	2730^{0}C	Melting Point	2072^{0}C
Magnetic Susceptibility	-12.8 X 10^{-6} cm^3/mol	Form	Powder
Molar Mass	40.11 gm/mol	Molar Mass	101.96 gm/mol
Hardness	162 HRC	Purity	99.90%
Purity	99.50%	Particle Size	20 Micron
Form	Powder		
Particle Size	20 Micron		

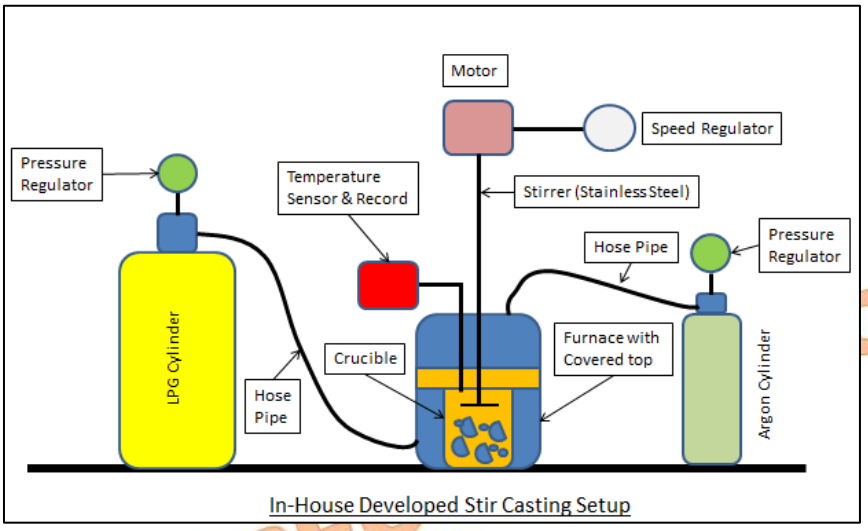

Fig.01 Schematic diagram of stir casting setup

In order to develop the magnesium alloy-based composite, a controlled environment of inert gas has been used. In order to validate the manufactured sample, an Energy Dispersive X-ray Spectroscopy (EDS) test has been conducted at the Electron Microscopy lab, Advanced Centre for Material Science, Indian Institute of Technology Kanpur. At random places, four areas were selected for observations. Results obtained show the presence of Al and Si particles in the developed samples. These compositional values are more than the values of Al and Si present in the purest form of AZ91 Alloy as obtained from the supplier. Figure 01 (a-d) shows the graphs and values obtained during the EDS test. It reveals the inclusion of Alumina and Silica in magnesium alloy, hence validating the sample.

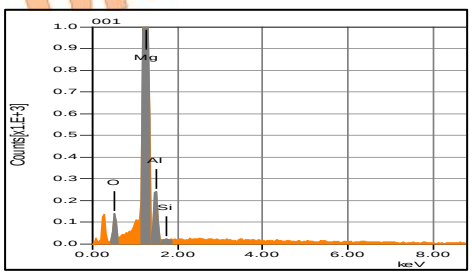

Fig.01 (a) EDS graph of area 01

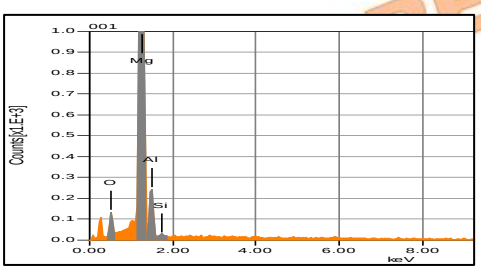

Fig. 01 (b) EDS graph of area 02

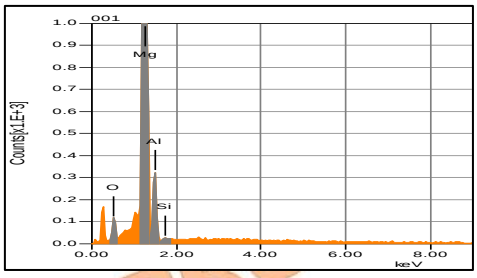

Fig.01 (c) EDS graph of area 03

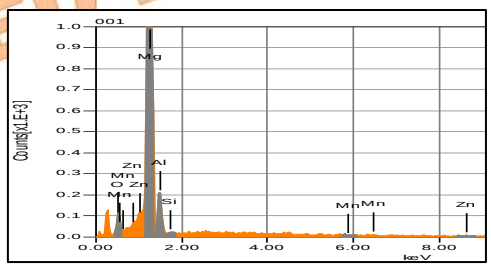

Fig. 01 (d) EDS graph of area 04

Developed composite samples have been analysed for SEM microstructure as shown in Figure 01(e) & 01(f). Figure 01(e) shows the α-Mg of AZ91 as a light grey area. Reinforcement of SiC and Alumina can be seen as a dark grey area. Grain boundaries have also been observed. In Figure 01(f) generation of micro-cracks has been observed. It may be due to shrinkage stress or thermal mismatch during cooling. It may be a potential region of failure under load conditions.

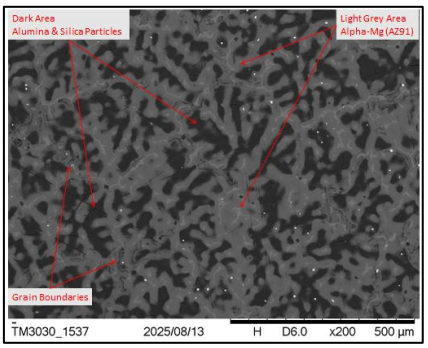

Fig.01 (e) SEM image @200x

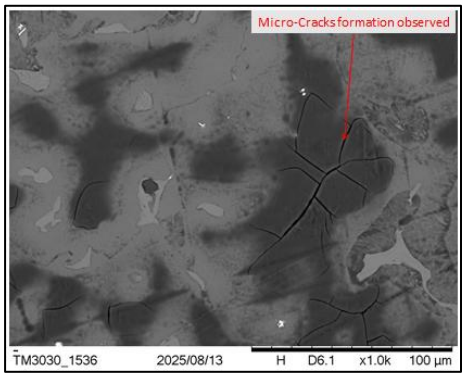

Fig.01 (f) SEM image @1000x

2.2 Machining Setup and Process Parameters:

The complete machining of the developed Mg/SiCp/Al_2O_3p hybrid metal matrix composite was carried out on a CNC WIRE CUT EDM Machine, Express cut series, Model: EX-4050C, as shown in Figure 02. Machining was performed using a molybdenum wire electrode. It has a diameter of 0.18 mm, and it is reusable. It has a maximum wire speed of 10.4 m/s. The width of the slot removed from the sample is 2mm. Commercially available deionized water is used as a dielectric fluid. It is used as a medium to complete the machining process and to remove the debris from the slot. To determine the levels of input parameters needed to carry out the research, pilot tests were carried out.

Fig. 02: CNC WEDM M/c

Fig.03: Machined sample

Input parameters for machining, T_{on}, T_{off}, I & WS, were varied with three different levels. Other process variables, such as dielectric medium concentration, wire tension, dielectric flow pressure, cutting voltage, and voltage fluctuation, were kept constant for all the experiments. Table 03 depicting the input machining parameters and their levels used for machining the developed samples.

Table 03: Assigned machining parameters and their different levels

Machining Variables	Symbol	Units	Levels		
			1	2	3
Pulse-on-Time	T_{on}	µs	6	18	30
Pulse-off-Time	T_{off}	µs	5	7	9
Current	I	Ampere	1	3	5
Wire Speed	WS	m/sec	3.12	6.76	10.4

2.3 Measurements and Calculations:

CNC wire-cut EDM was used to machine the samples. A molybdenum wire electrode was used as a cutting tool to cut the slots in the specimen. After that machining slots were analysed for geometrical errors. Kerf width (Top surface and Bottom surface) and taper angle are analysed. Kerf geometry was measured using an optical microscope (Model: DP 22, make: Olympus, magnification of 10×) at the Centre of Advanced Studies, Lucknow, as shown in Figure 05. The ImageJ tool is also used to calculate the kerf width.

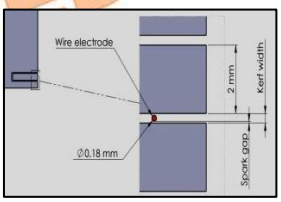

Fig.4: Kerf geometry of slot

Fig.5: Optical microscope

Kerf width is used to determine the dimensional accuracy of the finishing product. Spark gap is the distance between the wire electrode and the workpiece surface. Kerf width is the width of the slot produced during the erosion process. Development of the kerf width was also caused by vibrations in the tool and tool wear as well. Figure 04 shows the kerf geometry. Kerf width is calculated as per equation 1.

$$Kerf\ Width = \frac{(Total\ width\ of\ slot - Width\ of\ slot\ removed)}{2} \quad \ldots Eqn(1)$$

The following Figure 04(a, b & c) represents the images of the machined sample for the measurement of Bottom kerf width, and Figure 04(d, e & f) represents the images for measurements of Top kerf width.

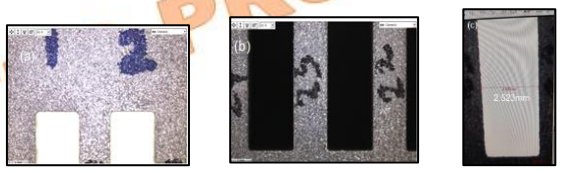

Fig. 04(a, b & c): Bottom kerf width

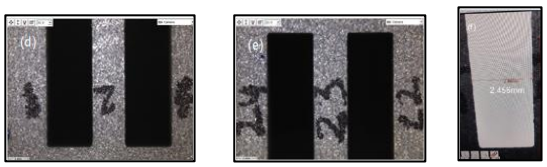

Fig. 04(d, e & f): Top kerf width

Taper Angle is calculated by taking the difference between the top kerf width and the bottom kerf width. Taper angle is defined as the deviation produced during the cutting of the slot. It is an angle by which the top surface and

the bottom surface of the cut slot deviates with each other. It is represented as θ. Taper angle has been calculated as per equation 2.

$$Tan\ \theta = \frac{T_{kw} \sim B_{kw}}{\text{Thickness of sample}} \quad \ldots\ldots Eqn(2)$$

3. Design of Experiments using RSM Approach

The RSM is a widely used tool for modelling statistical data to establish the correlation between the input machining parameters and output variables. RSM approach has two variants in methodology, Central Composite type Design (CCD) & Box – Behnken type Design (BBD). In the present work, RSM with the BBD approach is used to design the experiments. Table 03 of input parameters is used to develop the experimentation model using the MINITAB-18 software, as shown in table 04.

Table 04: Design of experiments for machining the sample

Exp. No. (Run)	T_{on} (µs)	T_{off} (µs)	I (A)	WS (m/s)
1	6	5	3	6.76
2	30	5	3	6.76
3	6	9	3	6.76
4	30	9	3	6.76
5	18	7	1	3.12
6	18	7	5	3.12
7	18	7	1	10.40
8	18	7	5	10.40
9	6	7	3	3.12
10	30	7	3	3.12
11	6	7	3	10.40
12	30	7	3	10.40
13	18	5	1	6.76
14	18	9	1	6.76
15	18	5	5	6.76
16	18	9	5	6.76
17	6	7	1	6.76
18	30	7	1	6.76
19	6	7	5	6.76
20	30	7	5	6.76
21	18	5	3	3.12
22	18	9	3	3.12
23	18	5	3	10.40
24	18	9	3	10.40
25	18	7	3	6.76
26	18	7	3	6.76
27	18	7	3	6.76

4. Results and Discussion

Samples of AZ91/SiCp/Al_2O_3p hybrid MMMC were machined on CNC-WEDM according to the DOE obtained through the RSM-BBD approach. The following Table 05 shows the calculations of top kerf width, bottom kerf width, and taper angle made after the machining of the sample. Taper angle shows the deviation between the upper and bottom surfaces. Positive (+) sign indicates the clockwise direction and negative (-) sign denotes the anti-clockwise direction of taper angle.

Table 05: Calculations of kerf width & taper angle of machined sample

Run	Top Kerf Width (T_{kw}) (mm)	Bottom Kerf Width (B_{kw}) (mm)	Taper Angle (θ^0)
1	0.188	0.169	+ 0.108
2	0.201	0.190	+ 0.063
3	0.175	0.169	+ 0.034
4	0.178	0.184	- 0.034
5	0.183	0.169	+ 0.080
6	0.198	0.184	+ 0.080
7	0.189	0.169	+ 0.114
8	0.202	0.181	+ 0.120
9	0.162	0.172	- 0.057
10	0.189	0.187	+ 0.011
11	0.174	0.190	- 0.091
12	0.206	0.206	0.000
13	0.168	0.184	- 0.091
14	0.173	0.169	+ 0.022
15	0.193	0.186	+ 0.040
16	0.193	0.189	+ 0.022
17	0.148	0.179	- 0.177
18	0.177	0.188	- 0.063
19	0.173	0.191	- 0.103
20	0.189	0.187	+ 0.011
21	0.183	0.188	- 0.028
22	0.183	0.180	+ 0.017
23	0.180	0.198	- 0.103
24	0.189	0.182	+ 0.040
25	0.192	0.182	+ 0.057
26	0.189	0.182	+ 0.040
27	0.196	0.187	+ 0.051

4.1 Effect of input parameters on top kerf width and its variations

An analysis of variance (ANOVA) was conducted to evaluate the significance of process parameters on the response variable. The overall model was found to be marginally significant (P = 0.094), explaining 71.62% of the total variation in the response. Among the linear terms, pulse-on time (T_{on}) and current (I) showed a statistically significant effect on the

response with P-values of 0.005 and 0.009, respectively, indicating their dominant influence. The quadratic term for T_{on} was marginally significant (P = 0.057), suggesting a non-linear relationship. The lack-of-fit test showed marginal significance (P = 0.096). Overall, the results suggest that optimizing Ton and current is critical for improving the process performance.

Top kerf width (T_{kw}) was evaluated using four input parameters through 27 experimental runs based on the RSM-BBD design. T_{kw} ranged between 0.148–0.206 mm, with the optimum value of 0.180 mm obtained at T_{on} = 18µs, T_{off} = 5µs, I = 3A, and WS = 10.4m/s, while the maximum value of 0.206mm occurred at T_{on} = 30µs, T_{off} = 7µs, I = 3A, and WS = 10.4 m/s.

ANOVA and response plots (Figures 06–07) indicate that T_{on} and current are the most significant factors influencing T_{kw}, while T_{off} and wire speed showed comparatively minor effects. T_{kw} increased with T_{on} and current up to an optimum, decreased with T_{off}, and showed a positive correlation with wire speed.

Table 06: ANOVA for T_{kw} of AZ91/SiCp/Al_2O_3p hybrid MMMC

Source	DF	Seq SS	Contribution	Adj SS	Adj MS	F-Value	P-Value
Model	14	0.003127	71.62%	0.003127	0.000223	2.16	0.094
Linear	4	0.002396	54.86%	0.002396	0.000599	5.80	0.008
T_{on}	1	0.001200	27.48%	0.001200	0.001200	11.62	0.005
T_{off}	1	0.000040	0.92%	0.000040	0.000040	0.39	0.544
I	1	0.001008	23.09%	0.001008	0.001008	9.76	0.009
WS	1	0.000147	3.37%	0.000147	0.000147	1.42	0.256
Square	4	0.000631	14.44%	0.000631	0.000158	1.53	0.256
T_{on}*T_{on}	1	0.000365	8.36%	0.000456	0.000456	4.42	0.057
T_{off}*T_{off}	1	0.000036	0.83%	0.000075	0.000075	0.73	0.411
I*I	1	0.000228	5.23%	0.000192	0.000192	1.86	0.198
WS*WS	1	0.000001	0.03%	0.000001	0.000001	0.01	0.911
2-Way Interaction	6	0.000101	2.31%	0.000101	0.000017	0.16	0.982
T_{on}*T_{off}	1	0.000025	0.57%	0.000025	0.000025	0.24	0.632
T_{on}*I	1	0.000042	0.97%	0.000042	0.000042	0.41	0.534
T_{on}*WS	1	0.000006	0.14%	0.000006	0.000006	0.06	0.810
T_{off}*I	1	0.000006	0.14%	0.000006	0.000006	0.06	0.810
T_{off}*WS	1	0.000020	0.46%	0.000020	0.000020	0.20	0.666
I*WS	1	0.000001	0.02%	0.000001	0.000001	0.01	0.923
Error	12	0.001239	28.38%	0.001239	0.000103		
Lack-of-Fit	10	0.001215	27.82%	0.001215	0.000121	9.85	0.096
Pure Error	2	0.000025	0.56%	0.000025	0.000012		
Total	26	0.004367	100.00%				

Table 07: Model summary for T_{kw} of AZ91/SiCp/Al_2O_3p hybrid MMMC

S	R-sq	R-sq(adj)	PRESS	R-sq(pred)
0.0101626	71.62%	38.51%	0.0070520	0.00%

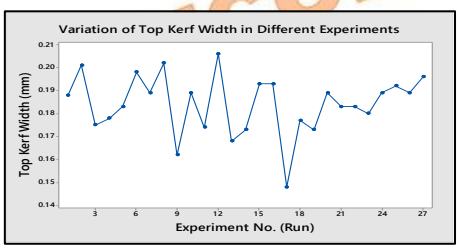

Fig.06: Variation of T_{kw} during different runs

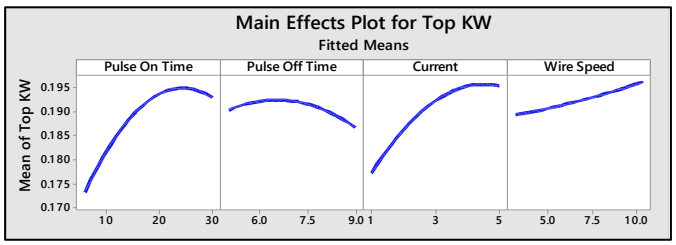

Fig. 07: Effect of input parameters on T_{kw}

4.2 Effect of input parameters on bottom kerf width and its variations

The model was statistically marginal with a P-value of 0.084, yet explained a substantial proportion of the response variability, with an R^2 of 72.38%. The adjusted R^2 was 40.16%, reflecting the model's explanatory power after accounting for the number of predictors. The standard error of the regression (S) was 0.0100, and the predicted R^2 was 0.00%, indicating that the model fits the experimental data reasonably well. Among the linear terms, pulse-on time (T_{on}) and current (I) were statistically significant with P-values of 0.004 and 0.009, respectively, and together accounted for more than 50% of the model's total contribution. The quadratic term T_{on}*T_{on} was marginally significant (P = 0.055).

Bottom kerf width (B_{kw}) obtained through the RSM-BBD design showed critical variations across experiments, ranging from 0.169–0.206 mm. The optimum value of 0.169 mm was achieved at T_{on} = 18 µs, T_{off} = 9 µs, I = 3 A, and WS = 3.12 m/s, while the maximum of 0.206 mm occurred at T_{on} = 30 µs, T_{off} = 7 µs, I = 3 A, and WS = 10.4 m/s. Parametric influence plots (Figures 08–09) revealed that B_{kw} increases exponentially with T_{on} and positively with wire speed, though less steeply. Increasing T_{off} reduces B_{kw}, while current influences it following a square-root type trend.

Table 08: ANOVA for B_{kw} of AZ91/SiCp/Al_2O_3p hybrid MMMC

Source	DF	Seq SS	Contribution	Adj SS	Adj MS	F-Value	P-Value
Model	14	0.003161	72.38%	0.003161	0.000226	2.25	0.084
Linear	4	0.002425	55.52%	0.002425	0.000606	6.03	0.007
T_{on}	1	0.001240	28.40%	0.001240	0.001240	12.34	0.004
T_{off}	1	0.000040	0.92%	0.000040	0.000040	0.40	0.538
I	1	0.000990	22.67%	0.000990	0.000990	9.85	0.009
WS	1	0.000154	3.53%	0.000154	0.000154	1.53	0.239
Square	4	0.000625	14.32%	0.000625	0.000156	1.56	0.249
T_{on}*T_{on}	1	0.000359	8.21%	0.000452	0.000452	4.50	0.050
T_{off}*T_{off}	1	0.000034	0.77%	0.000073	0.000073	0.73	0.410
I*I	1	0.000232	5.32%	0.000197	0.000197	1.96	0.186
WS*WS	1	0.000001	0.02%	0.000001	0.000001	0.01	0.925
2-Way Interaction	6	0.000111	2.55%	0.000111	0.000019	0.18	0.976
T_{on}*T_{off}	1	0.000036	0.82%	0.000036	0.000036	0.36	0.561
T_{on}*I	1	0.000042	0.97%	0.000042	0.000042	0.42	0.529
T_{on}*WS	1	0.000006	0.14%	0.000006	0.000006	0.06	0.807
T_{off}*I	1	0.000006	0.14%	0.000006	0.000006	0.06	0.807
T_{off}*WS	1	0.000020	0.46%	0.000020	0.000020	0.20	0.662
I*WS	1	0.000000	0.01%	0.000000	0.000000	0.00	0.961
Error	12	0.001206	27.62%	0.001206	0.000101		
Lack-of-Fit	10	0.001182	27.06%	0.001182	0.000118	9.58	0.098
Pure Error	2	0.000025	0.56%	0.000025	0.000012		
Total	26	0.004368	100.00%				

Table 09: Model summary for B_{kw} of AZ91/SiCp/Al_2O_3p hybrid MMMC

S	R-sq	R-sq(adj)	PRESS	R-sq(pred)
0.0100267	72.38%	40.16%	0.0068624	0.00%

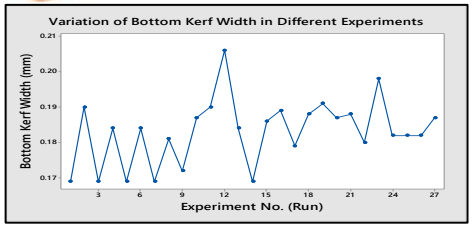

Fig. 08: Variation of B_{kw} during different runs

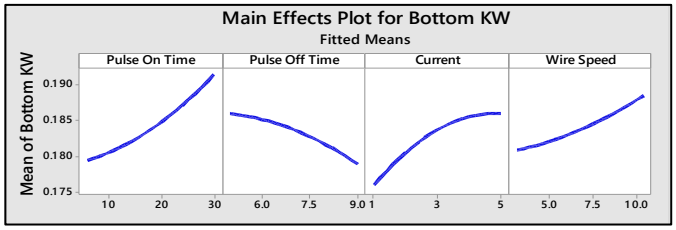

Fig.09: Effect of input parameters on bottom kerf width

4.3 *Effect of input parameters on taper angle and its variations*

The ANOVA results revealed that the quadratic regression model was statistically significant (F = 2.90, p = 0.036) and explained 77.18% of the total variation in the response. Among the process parameters, pulse-on time (T_{on}) and current (I) were the most influential, with Ton showing both significant linear (p = 0.010) and quadratic (p = 0.009) effects, indicating a strong nonlinear influence and the existence of an optimal range. Current also exhibited a significant effect (p = 0.004), confirming its critical role in process performance. The model summary further supports these findings. The residual standard deviation was low (S = 0.0088), confirming a good fit between experimental and predicted values. The coefficient of determination (R^2 = 77.18%) indicates a strong overall fit, but the adjusted R^2 of 50.56% reflects the influence of several non-significant terms in the model.

Taper angle, representing deviation between upper and lower edges, was evaluated using RSM-BBD experiments and plotted in Figure 10. Values ranged from +0.1140° (clockwise, Exp. 07) to −0.1770° (anticlockwise, Exp. 17), with the optimum value of 0.000° achieved at T_{on} = 30 µs, T_{off} = 7 µs, I = 3 A, and WS = 10.4 m/s, indicating a straight cut. Input parameter effects (Figure 11) showed taper angle is highly sensitive to T_{on}, increasing initially and then reducing after a threshold, while T_{off} and current exhibited similar but less pronounced trends. Wire speed showed only a marginal influence.

Table 10: ANOVA for TA of AZ91/SiCp/Al_2O_3p hybrid MMMC

Source	DF	Seq SS	Contribution	Adj SS	Adj MS	F-Value	P-Value
Model	14	0.003157	77.18%	0.003157	0.000226	2.90	0.036
Linear	4	0.001927	47.10%	0.001927	0.000482	6.19	0.006
T_{on}	1	0.000736	18.00%	0.000736	0.000736	9.47	0.010
T_{off}	1	0.000016	0.40%	0.000016	0.000016	0.21	0.655
I	1	0.000990	24.20%	0.000990	0.000990	12.73	0.004
WS	1	0.000184	4.50%	0.000184	0.000184	2.37	0.150
Square	4	0.001125	27.51%	0.001125	0.000281	3.62	0.037
T_{on}*T_{on}	1	0.000667	16.30%	0.000752	0.000752	9.67	0.009
T_{off}*T_{off}	1	0.000250	6.11%	0.000252	0.000252	3.24	0.097
I*I	1	0.000182	4.44%	0.000120	0.000120	1.55	0.237
WS*WS	1	0.000027	0.66%	0.000027	0.000027	0.35	0.567
2-Way Interaction	6	0.000105	2.57%	0.000105	0.000018	0.23	0.961
T_{on}*T_{off}	1	0.000036	0.88%	0.000036	0.000036	0.46	0.509
T_{on}*I	1	0.000042	1.03%	0.000042	0.000042	0.54	0.475
T_{on}*WS	1	0.000000	0.01%	0.000000	0.000000	0.00	0.956
T_{off}*I	1	0.000006	0.15%	0.000006	0.000006	0.08	0.782
T_{off}*WS	1	0.000020	0.50%	0.000020	0.000020	0.26	0.619
I*WS	1	0.000000	0.01%	0.000000	0.000000	0.00	0.956
Error	12	0.000933	22.82%	0.000933	0.000078		
Lack-of-Fit	10	0.000909	22.22%	0.000909	0.000091	7.37	0.125
Pure Error	2	0.000025	0.60%	0.000025	0.000012		
Total	26	0.004091	100.00%				

Table 11: Model summary for TA of AZ91/SiCp/Al_2O_3p hybrid MMMC

S	R-sq	R-sq(adj)	PRESS	R-sq(pred)
0.0088196	77.18%	50.56%	0.0052899	0.00%

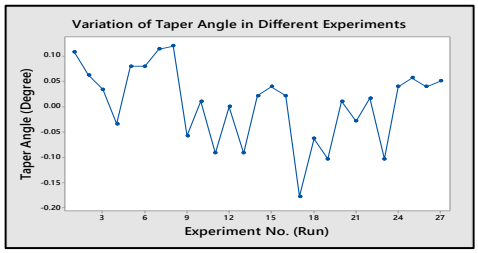

Fig.10: Variation of TA during different runs

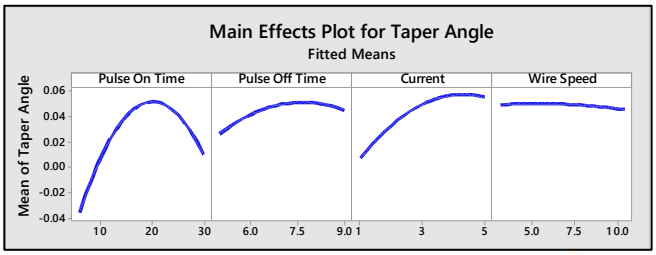

Fig 11: Effect of input parameters on Taper Angle

In the present study, the effect of input parameters on dimensional accuracy was assessed. The top kerf width varied between 0.148 mm (148 µm) and 0.206 mm (206 µm), which is significantly lower than the 335 µm reported by V.H. Chaitanya et al. [38] for EDM of Mg alloy at higher pulse-on times. This indicates that the addition of SiC and Al_2O_3 reinforcements increases brittleness and improves dimensional accuracy. The bottom kerf width ranged from 0.169 mm (169 µm) to 0.206 mm (206 µm), which is about 34% lower than the optimum 0.316 mm kerf width reported by A. Munippan et al. [39] for AZ91 Mg alloy, highlighting the improved dimensional stability of the reinforced composites. Similar to the findings of M.K. Debta et al. for AZ91D alloy [WEDM], the current study also observed an initial increase in kerf width and taper angle with increasing pulse-on time, followed by a decrease at higher values.

The observed trends can be attributed to the discharge mechanism. At lower pulse-on times, higher discharge energy increases erosion, widening the kerf. However, prolonged pulse durations cause unstable plasma channels, inefficient debris removal, recast layer formation, and resistance from reinforcements, thereby reducing kerf width. At the bottom surface, higher pulse-on time delivers more thermal energy per discharge, leading to greater erosion, while higher wire speed enhances flushing and fresh wire exposure, slightly increasing the bottom kerf.

Taper angle behavior showed that increasing pulse-on time and current initially raised taper due to localized energy concentration at the surface, but beyond a threshold, better energy distribution and spark penetration reduced taper. Pulse-off time exhibited a minor influence, while wire speed had a negligible effect, confirming that taper formation is primarily governed by discharge energy and its distribution along the cut depth.

5. Conclusions

The present work aimed to machine the AZ91-based hybrid composite with wire cut EDM, which has been completed successfully. Experiments were designed using research surface methodology with the BBD approach using Minitab-18 software. A total of 27 experiments have been performed on the sample. The following are the effective concluding points as per the work carried out.

1. The hybrid composite was successfully machined using wire EDM, and key dimensional parameters - Kerf width (Top & Bottom) and Taper angle were measured.
2. It has been found that, optimum value of top kerf width (0.180mm) is obtained at T_{on} = 18µs, T_{off} = 5µs, I = 3A & WS = 10.4m/s; optimum value of bottom kerf width (0.180mm) is obtained at T_{on} = 18µs, T_{off} = 9µs, I = 3A & WS = 3.12m/s and optimum value of taper angle (0.00^0) is obtained at T_{on} = 30µs, T_{off} = 7µs, I = 3A & WS = 10.4m/s.
3. It is evident from Table 05 and Figure 06 that an increase in pulse off time shows a decreasing trend for top kerf width, while on increasing other input parameters, top kerf width keeps on increasing.
4. It is found that pulse on time is the most critical factor for bottom kerf width, followed by wire speed.
5. In consideration of the taper angle, pulse on time, and current is most significant factors in deciding the taper angle and straightness of the machined sample.

Nomenclature:

MMC	Metal Matrix Composite
WEDM	Wire Electric Discharge Machining
RSM	Response Surface Methodology
BBD	Box Behnken Design
ANOVA	Analysis of Variance
T_{on}	Pulse-on-Time
T_{off}	Pulse-off-Time
I	Current
WS	Wire Speed
T_{kw}	Top Kerf Width
B_{kw}	Bottom Kerf Width
TA	Taper Angle

Acknowledgements:

The authors wish to acknowledge the Faculty of Mechanical Engineering, Institute of Technology, SRMU, Lucknow, for providing registration number 202010102000001, and the Advanced Center for Material Science, Indian Institute of Technology, Kanpur & Centre for Advanced Studies, Lucknow, for providing testing facility.

Author's Contribution:

Dheeraj Kumar- Setup development, Experimentation, Resources, Conceptualization, Validation, Data Collection, Writing Manuscript;

Rajesh Kumar Porwal- Supervision, Writing- Review & Editing.

Funding:

The authors declare that no funding was received during experimentation & preparation of this manuscript.

Conflict of Interests:

The authors declare no conflict of interest in relevance to financial or non-financial aids.

References

[1]. Kumar D, Porwal RK. Recent Advances in Machining of Composite Materials by Electrical Discharge Machine. Key Engineering Materials, November 2023; Volume 965: pages 3–20. https://doi.org/10.4028/p-tsff0o.

[2]. Kashif Ishfaq, Sadaf Zahoor, Sarmad Ali Khan, Mudassar Rehman, Abdullah Alfaify, Saqib Anwar, Minimizing the corner errors (top and bottom) at optimized cutting rate and surface finish during WEDM of Al6061, Engineering Science and Technology, an International Journal, Volume 24, Issue 4, 2021, Pages 1027-1041, ISSN 2215-0986, https://doi.org/10.1016/j.jestch.2021.01.008.

[3]. Muthu kumar V, Suresh babu A, Venkatasamy R, Raajenthiren M. Optimization of the WEDM parameters on machining Incoloy 800 super alloy with multiple quality characteristics. Int J Eng Sci Technol 2010; 2:1538–47.

[4]. Naveed, R., Mufti, N.A., Ishfaq, K. et al. Complex taper profile machining of WC-Co composite using wire electric discharge process: analysis of geometrical accuracy, cutting rate, and surface quality. Int J Adv Manuf Technol 105, 411–423 (2019). https://doi.org/10.1007/s00170-019-04150-x

[5]. W.U. Xiaoyu, Shujuan, Experimental investigation of hybrid machining combining wire electrical discharge machining WEDM and fixed abrasive wire saw, Int. J. Adv. Manuf. Technol. 95 5 (8) (2017) 2613–2623.

[6]. N.R.J. Hynes, A.D. Asirvatham, R. Sankaranarayanan, S. Raja, B. Benita, J. Atchaya, Investigation on surface roughness and kerf analysis in abrasive water jet machining of silicon carbide, Archives of Materials Science and Engineering 120/1 (2023) 30-35. DOI: https://doi.org/10.5604/01.3001.0053.6017.

[7]. Baliarsingh AK, Samantaray MK. Analysis of Wire-Cut Electro Discharge Machining of Polymer Composite Materials, Dogo Rangsang Research Journal ISSN : 2347-7180 Vol-08 Issue-14 No. 04, April 2021.

[8]. Anshuman Kumar, Ph D.Thesis titled 'Investigations on Machining Aspects of Inconel 718 during Wire Electro-Discharge Machining (WEDM): Experimental and Numerical analysis' submitted at National Institute of Technology, Rourkela, November 2016.

[9]. Muhammad W, Iqbal SA, Khan YA, Muhammad T. Analysis and Multi-Objective Optimization of Wire Cut Process Parameters for Efficient Cutting of Tapered Carbon Steels Using Wire EDM. Journal of Engineering Research. 2021 Nov 3.

[10]. Majumder, H., Maity, K.P. Predictive Analysis on Responses in WEDM of Titanium Grade 6 Using General Regression Neural Network (GRNN) and Multiple Regression Analysis (MRA). Silicon 10, 1763–1776 (2018). https://doi.org/10.1007/s12633-017-9667-1

[11]. Farooq, M.U.; Anwar, S.; Kumar, M.S.; AlFaify, A.; Ali, M.A.; Kumar, R.; Haber, R. A Novel Flushing Mechanism to Minimize Roughness and Dimensional Errors during Wire Electric Discharge Machining of Complex Profiles on Inconel 718. Materials 2022, 15, 7330. https://doi.org/10.3390/ma15207330.

[12]. Ablyaz, T.R.; Shlykov, E.S.; Muratov, K.R.; Sidhu, S.S. Analysis of Wire-Cut Electro Discharge Machining of Polymer Composite Materials. Micromachines 2021, 12, 571. https://doi.org/10.3390/mi12050571.

[13]. Shah A, Mufti NA, Rakwal D, Bamberg E (2011) Material removal rate, kerf, and surface roughness of tungsten carbide machined with wire electrical discharge machining. J Mater Eng Perform 20(1):71–76.

[14]. Naveed, R., Mufti, N.A., Mughal, M.P. et al. Machining of curved profiles on tungsten carbide-cobalt composite using wire electric discharge process. Int J Adv Manuf Technol 93, 1367–1378 (2017).

https://doi.org/10.1007/s00170-017-0592-7.

[15]. Vijaya Raja Ragavan G, Poovazhagan Lakshmanan and Mariyappan Mahalingam; Examining the surface roughness and kerf quality of micro-slots cut on the surfaces of Ti-B4C nanocomposites by WEDM: a desirability approach, Materials Research Express, Volume 9, Number 12, 2022, doi: 10.1088/2053-1591/acadd2.

[16]. Kolli, M., Ram Prasad, A.V.S. & Naresh, D.S. Multi-objective optimization of AAJM process parameters for cutting of B4C/Gr particles reinforced Al 7075 composites using RSM-TOPSIS approach. SN Appl. Sci. 3, 711 (2021). https://doi.org/10.1007/s42452-021-04699-x.

[17]. Pramanik A, Basak AK, Prakash C (2019) Understanding the wire electrical discharge machining of Ti6Al4V alloy. Heliyon 5(4):1–17. https://doi.org/10.1016/j.heliyon.2019.e01473.

[18]. Bineet Pal Singh, Jaswinder Singh, Jaspreet Singh, Mohit bhayana, Deepam Goyal, Experimental investigation of machining nimonic-80A alloy on wire EDM using response surface methodology, Metal Powder Report, Volume 76, Supplement 1, 2021, Pages S9-S17, ISSN 0026-0657, https://doi.org/10.1016/j.mprp.2020.12.001.

[19]. Moharana, B.R., Behera, B.C., Syed, S.A., Muduli, K., Barnwal, S. (2023). Experimental Investigation of Machining NIMONIC 80 Alloy by WEDM Process via Multi-objective Optimisation Techniques: A Sustainable Approach. In: Kandasamy, J., Sakthivel, A.R., Davim, J.P. (eds) Progress in Sustainable Manufacturing. Management and Industrial Engineering. Springer, Singapore. https://doi.org/10.1007/978-981-99-0201-9_6.

[20]. C. Thiagarajan, T. Maridurai, T. Shaafi, A. Muniappan, Machinability studies on hybrid nano-SiC and nano-ZrO2 reinforced aluminium hybrid composite by wire-cut electrical discharge machining, Materials Today: Proceedings, Volume 80, Part 3, 2023, Pages 2731-2739, ISSN 2214-7853, https://doi.org/10.1016/j.matpr.2021.07.029.

[21]. Kumar, B.K., Das, V.C. Study and parameter optimization with AISI P20 + Ni in Wire EDM performance using RSM and hybrid DBN based SAR. Int J Interact Des Manuf 17, 679–701 (2023). https://doi.org/10.1007/s12008-022-00991-1.

[22]. Naveed, R., Ishfaq, K., Harris, M. et al. WEDM of tapered rectangular geometry in tungsten–carbide cobalt composite (WC–Co): geometrical errors and surface roughness analysis. J Braz. Soc. Mech. Sci. Eng. 45, 67 (2023). https://doi.org/10.1007/s40430-022-03945-6.

[23]. Bisaria, H., Rouniyar, A.K. Processing of Triangular Profile on Inconel-825 Superalloy by Wire Electrical Discharge Machining and Corner Error Optimization Using Teaching Learning-Based Optimization Technique. J. of Materi Eng and Perform (2023). https://doi.org/10.1007/s11665-022-07797-y.

[24]. Lakshmanan S, Rajendran R, Shanmugakani SK, Krishnamoorthy V. Analyzing the geometrical errors of silicon nitride-titanium nitride on performing electric discharge machining using response surface methodology. Proceedings of the Institution of Mechanical Engineers, Part E: Journal of Process Mechanical Engineering. 2023;0 (0). Doi: 10.1177/09544089231166303.

[25]. B.P. Singh, J. Singh, J. Singh, M. Bhayana, K. Singh, Rajesh Singh, Experimental examination of the machining characteristics of Nimonic 80-A alloy on wire EDM, Materials Today: Proceedings, Volume 69, Part 2, 2022, Pages 291-296, ISSN 2214-7853, https://doi.org/10.1016/j.matpr.2022.08.537.

[26]. Sahu A, Pattanayak S, Panda S. WEDM microdrilling of 316 L stainless steel orthopedic implant. Proceedings of the Institution of Mechanical Engineers, Part C: Journal of Mechanical Engineering Science. 2020;234(17):3416-3435. doi:10.1177/0954406220936302.

[27]. Arif, U., Khan, I.A. & Hasan, F. Thermal Modeling and Parametric Optimization for Machining of Aluminum (Al-10%SiCmicro-SiCnano)-Based Hybrid Composite Using Spark Erosion. J. of Materi Eng and Perform 34, 330–355 (2025). https://doi.org/10.1007/s11665-023-09042-6.

[28]. Umair Arif, Imtiaz Ali Khan, Faisal Hasan, Parametric analysis of the thermal model of electric discharge machining of Al-10%SiCmicro-SiCnano hybrid composites, Materials Today: Proceedings, 2023, ISSN 2214-7853, https://doi.org/10.1016/j.matpr.2023.06.346.

[29]. Umair Arif, Imtiaz ali Khan, Faisal Hasan, Afsar Husain, Sanan H. Khan, Effects of EDM parameters on residual stress and microhardness in Al-10 %SiCmicro-SiCnano hybrid composites: A Simulation and Experimental study, Results in Engineering, Volume 26, 2025, 105353, ISSN 2590-1230,

https://doi.org/10.1016/j.rineng.2025.105353.
[30]. Mahamood Ansari, Imtiaz Ali Khan, Umair Arif, Finite element analysis of wire EDM process parameters on performance characteristics of Al–SiC hybrid composite with micro and nano reinforcements, Hybrid Advances, Volume 6, 2024, 100202, ISSN 2773-207X, https://doi.org/10.1016/j.hybadv.2024.100202.
[31]. Mustu, M., Demir, B., Aydin, F. et al. An Investigation on Powder-Mixed Electric Discharge Machining of TiB2 and Nanographene-Doped ZK60 Mg Matrix Composites. Arab J Sci Eng (2024). https://doi.org/10.1007/s13369-024-09737-5.
[32]. Dash D, Devarajaiah D, Dash SK, Samanta S, Rai RN. Experimental investigation and machining analysis of Mg/TiC composites during EDM. Composite Theory and Practice. 2024 Mar 31; 24 (1):9-16.
[33]. Ammisetti DK, Kruthiventi SH. Experimental analysis and artificial neural network teaching–learning-based optimization modeling on electrical discharge machining characteristics of AZ91 composites. Journal of Materials Engineering and Performance. 2024 Nov;33(21):11718-35.
[34]. Urtekin, L., Yılan, F., Şahin, İbrahim B., & Gök, K. (2025). Analysis of surface roughness and machining performance of AZ91 magnesium alloy cut by WEDM. Acta Polytechnica, 65(3), 361–370. https://doi.org/10.14311/AP.2025.65.0361.
[35]. Ikedue MC, Rajan J, Jose S, Oke S, Adedeji WO. Optimization of Wire Electrical Discharge Machining Process Parameters in AZ91 Magnesium Alloy Using Taguchi-Based Fuzzy Analytic Hierarchy Process (TFAHP) Method : doi: 10.14456/mijet.2024.2. Engineering Access [internet]. 2024 Feb. 19 [cited 2025 Aug. 9];10(1):6-20. available from: https://ph02.tci-thaijo.org/index.php/mijet/article/view/247497.
[36]. Kumar, D., Porwal, R.K. Parametric Optimization of Thermoelectric Machining of Stir-Cast Hybrid Magnesium Metal Matrix Composite with Alumina and Silicon Carbide as Reinforcement. J. Inst. Eng. India Ser. D 105, 1927–1943 (2024). https://doi.org/10.1007/s40033-023-00628-x.
[37]. Mohanavel V, Singh RP, Sekar S, Venkatesh R, Vaidyanathan IM, Ali M. Investigation of Al/Mg composite behaviour by the adaptation of SiC and Al2O3 nanoparticle via electromagnetic stir cast route. Materials Science and Technology. 2025;0(0). doi:10.1177/02670836241306686.
[38]. Vempati Harish Chaitanya, Prithivirajan Sekar, S. Narendranath, V. Balaji, A study on the influence of WEDM parameters on surface roughness, kerf width, and corrosion behavior of AZ31B Mg alloy, Materials Today: Proceedings, 2022, ISSN 2214-7853, https://doi.org/10.1016/j.matpr.2022.12.151.
[39]. A Muniappan et al 2018 IOP Conf. Ser.: Mater. Sci. Eng. 402 012171, DOI 10.1088/1757-899X/402/1/012171.
[40]. Malaya Kumar Debta, Ravi Mishra, Manoj Masanta, Experimental investigation on the machining performance of AZ91D (90% Mg) alloy by wire-cut EDM, Materials Today: Proceedings, Volume 33, Part 8, 2020, Pages 5557-5560, ISSN 2214-7853, https://doi.org/10.1016/j.matpr.2020.03.540.
[41]. Aruna, M., Krishnan, A.M., Nagarajan, N. et al. Integration of Magnesium Fluoride and Nano Alumina–Silicon Carbide Actions on Properties of AZ91 Alloy Hybrid Nanocomposites. Inter Metalcast (2025). https://doi.org/10.1007/s40962-025-01617-4.
[42]. Xiaozhe Ge, Kaibo Nie, Kunkun Deng, Chao Xu, Shilei Wang, Effect of SiC particles on microstructure and mechanical properties of SiCp/AZ91 magnesium matrix composite brazed joint, Journal of Alloys and Compounds, Volume 1010, 2025, 177387, ISSN 0925-8388, https://doi.org/10.1016/j.jallcom.2024.177387.
[43]. Sudhagar, S., Gopal, P.M., Maniyarasan, M. et al. Multi-objective optimization of machining parameters for Si3N4–BN reinforced magnesium composite in wire electrical discharge machining. Int J Interact Des Manuf 18, 4787–4802 (2024). https://doi.org/10.1007/s12008-024-01777-3.